ADVANCED FUNCTIONAL MATERIALS
www.afm-journal.de

Extreme Elasticity Anisotropy in Molecular Glasses

Yu Cang, Zuyuan Wang, Camille Bishop, Lian Yu, M. D. Ediger, and George Fytas**

Glasses are generally assumed to be isotropic and there are no literature reports of elastic anisotropy for molecular glasses. However, as glasses formed by physical vapor deposition can be structurally anisotropic, it is of interest to investigate the elastic anisotropy in these materials. Micro-Brillouin light spectroscopy is used in several experimental geometries to determine the elastic stiffness tensors of three glass films of itraconazole vapor-deposited at substrate temperatures (T_{sub}) of 330, 315, and 290 K, respectively. Significant elastic anisotropy is observed and, in these glasses, the elastic anisotropy shows a strong correlation with the molecular orientation. The out-of-plane and in-plane Young's moduli of the high T_{sub} (330 K) sample, which features a predominantly vertical molecular orientation, exhibit a high anisotropy ratio of 2.2. The observed elastic anisotropy is much larger than those previously observed in liquid crystals and even many crystalline solids.

1. Introduction

While it is sometimes assumed that glasses must be isotropic, there are important examples of anisotropic glasses.[1] Often anisotropy improves the properties of glassy materials, such as in organic light emitting diodes, which are vapor-deposited glasses of organic semiconductors.[2] For this application, devices are more efficient when the transition dipoles of the emitting molecules lie in the plane of the device, as this allows more of the emitted light to leave the device in the desired direction.[3] For other applications, such as organic field-effect transistors, vertical orientation of rod-like molecules may orient the π–π stacking network in the plane of the device, leading to a beneficial anisotropic charge mobility.[4,5] Recent work has investigated the mechanism by which anisotropic glasses are prepared by physical vapor deposition (PVD).[6,7] Deposition conditions can be found such that rod-shaped molecules have a tendency to either stand up or lie down in the deposited glass.[7] For disk-shaped molecules, glasses can be deposited with the molecular plane aligned either parallel[3,8] or perpendicular[9] to the substrate. Even molecules with a nearly spherical shape can form anisotropic glasses, exhibiting a tendency toward molecular layering and polar alignment of the molecular dipoles.[10]

While anisotropic molecular orientation and the associated anisotropy in the index of refraction have been extensively investigated in vapor-deposited glasses,[3,7,8] little is known about the mechanical anisotropy of the glasses prepared with this method. On a practical level, this is of interest for flexible electronics. Here the in-plane modulus will determine the stress imposed on a glassy material upon bending deformation.[11] On a fundamental level, many questions about the connection between molecular orientation and elastic anisotropy in molecular glasses are almost unexplored. For example, does orientational order necessarily imply mechanical anisotropy? Even if one intuitively expects that anisotropic molecular orientation is a condition for elastic anisotropy in molecular glasses, to our knowledge there are no successful predictions of elastic anisotropy based upon molecular orientation.

As a first attempt to understand the connection between molecular orientation and elastic anisotropy, here we use the Brillouin light spectroscopy (BLS) technique[12,13] to determine the elastic anisotropy of three vapor-deposited glasses of itraconazole. For anisotropic materials, the elastic response is direction-dependent and described by an elastic tensor, which can contain up to 21 elastic constants. Experimental determination of the elastic tensor requires direction-controlled material displacements at sufficiently high frequencies to assure negligible dissipation and elastic behavior. In contrast to other approaches, such as AFM indentation[14] and the film buckling method,[15] BLS is a noncontact and noninvasive technique based on the inelastic scattering of light by thermally excited acoustic phonons. It is particularly suitable for determining the elastic properties of transparent samples because the wave vector **q** of the scattering phonon can be selectively oriented over a wide range of angles. BLS has been utilized to determine the elastic stiffness tensor of many materials, including biofibers,[12] hybrid stacks of organic and inorganic materials,[13] molecular liquid crystals,[16] and crystalline inorganic membranes.[17]

For this work, we prepared vapor-deposited glasses of itraconazole, a pharmaceutical with antifungal properties. Itraconazole is a rod-shaped molecule with equilibrium liquid crystal phases. Glasses of itraconazole were prepared by physical vapor deposition onto substrates held at different temperatures in

Dr. Y. Cang, Dr. Z. Wang, Prof. G. Fytas
Max Planck Institute for Polymer Research
Ackermannweg 10, Mainz 55128, Germany
E-mail: fytas@mpip-mainz.mpg.de
C. Bishop, Prof. L. Yu, Prof. M. D. Ediger
Department of Chemistry
University of Wisconsin-Madison
1101 University Avenue
Madison, WI 53706, USA
E-mail: ediger@chem.wisc.edu
The ORCID identification number(s) for the author(s) of this article can be found under https://doi.org/10.1002/adfm.202001481.

DOI: 10.1002/adfm.202001481

order to achieve a range of molecular orientations.[18] The samples were deposited at three substrate temperatures – 330, 315, and 290 K (herein referred to as high T_{sub}, medium T_{sub}, and low T_{sub}, respectively). As previously reported[18] the high T_{sub} itraconazole glass shows a strong tendency for the molecular long axis to be parallel to the surface normal, while nearly all the molecular long axes lie near to the substrate plane for the low T_{sub} glass. Micro-BLS measurements were performed in both the transmission and backscattering geometries to determine the five independent elastic constants of the three glasses.

For these vapor-deposited glasses of itraconazole, we find that the elastic constants are strongly influenced by the anisotropic structure of the samples. The high T_{sub} sample with strong vertical orientation has more than a factor of 2 difference between the in- and out-of-plane Young's moduli. The observed elastic anisotropy for this sample is much larger than that previously observed for liquid crystals and is larger than that observed for many 3D crystals. In contrast, the low T_{sub} glass had nearly isotropic elastic properties. To our knowledge, this is the first report of elastic anisotropy for vapor-deposited glasses. This work opens the way for a systematic investigation of the mechanical anisotropy of vapor-deposited organic semiconductors, with relevance for organic electronics. More fundamentally, this work raises the question of whether there is a limit to mechanical anisotropy for amorphous systems, and what that limit might be.

2. Results

2.1. Sample Structure

In order to provide the context for the elastic anisotropy results, we briefly recount the structure of the three itraconazole glasses studied here. Three different substrate temperatures were used to prepare vapor-deposited glasses of the rod-shaped itraconazole (**Figure 1**a, Section S1, Supporting Information) termed accordingly as high T_{sub} (330 K), medium T_{sub} (315 K), and low T_{sub} (290 K) samples. The substrate temperature T_{sub} controls the structure of the vapor-deposited glass through a surface equilibration mechanism that has been described elsewhere.[7,18,19] Figure 1b presents grazing-incidence wide-angle X-ray scattering (GIWAXS) data for itraconazole glasses deposited at the three substrate temperatures along with schematic illustrations of their structures. For the GIWAXS and BLS experiments, we utilize a coordinate system where the x_3 axis is along the substrate normal, as shown in Figure 1b, with orthogonal axes x_1 and x_2 lying in the plane of the sample. The glasses deposited at high T_{sub} and medium T_{sub} both show evidence for smectic layering, as indicated by the diffraction peaks along q_3 (at 0.2, 0.4, and 0.6 Å^{-1}). Scattering along q_{12} (at 1.4 Å^{-1}) for these samples provides evidence for vertical molecular orientations, with a stronger vertical orientation found in the high T_{sub} sample. In contrast, the low T_{sub} sample shows a horizontal molecular orientation and no indication of smectic layering. The GIWAXS patterns illustrate that molecular packing in PVD glasses can be tuned continuously by changing T_{sub} during deposition.

The orientation of itraconazole molecules in PVD glasses has been characterized by IR transmission[18] and these results are shown in Figure 1c. IR measurements are sensitive to the orientation of a transition dipole along the long axis of the itraconazole molecule (denoted by $\hat{\boldsymbol{n}}$ in Figure 1a). The average orientation of molecular long axes relative to the substrate normal is quantified by the average value of $\cos^2\phi$, where ϕ is the angle between $\hat{\boldsymbol{n}}$ and the surface normal (x_3 axis), and the S_z order parameter is based upon the second Legendre polynomial.[20] These values are shown in Figure 1c and **Table 1** (along with an approximate value for the average angle between the molecular long axis and the surface normal). For reference, S_z would equal unity if all the long axes were aligned with the surface normal; all long axes in the plane of the film would yield $S_z = 0.5$. Clearly the high T_{sub} sample has molecules with the long axes close to vertical while the low T_{sub} sample shows a strong tendency for the molecular long axis to lie in the sample plane. Table 1 also presents index of refraction (n_o = ordinary, n_e = extraordinary) values obtained with spectroscopic ellipsometry of the samples utilized for the BLS measurements. The birefringence ($\Delta n = n_e - n_o$) is also sensitive to the molecular orientation, with positive values indicating vertically oriented molecules.[18]

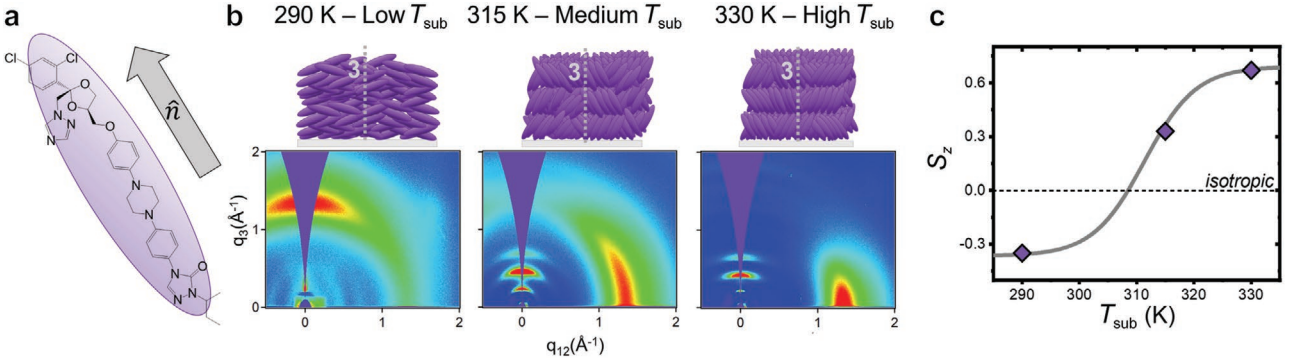

Figure 1. Grazing-incidence wide-angle X-ray scattering (GIWAXS) and molecular orientation for itraconazole glasses investigated in this work. a) Chemical structure of itraconazole, where $\hat{\boldsymbol{n}}$ indicates the orientation of the long molecular axis. b) GIWAXS of itraconazole on Si(100) at substrate temperatures used in this study, with illustrations of proposed structures. As the substrate temperature during deposition is increased, glasses are produced with nearest-neighbor packing that changes from localized out-of-plane of the substrate to in-plane. c) S_z, the orientation order parameter, showing the average orientation of the molecular long axes in the three glasses.

Table 1. Orientation order parameter and birefringence for the itraconazole glasses deposited at different substrate temperatures.

Sample	T_{sub} [K]	S_z (IR)[a)]	$\langle\cos^2\phi\rangle$	Avg. ϕ [°][b)]	n_o	n_e	$\Delta n = n_e - n_o$
High	330	0.67	0.78	28	1.565	1.715	0.150
Medium	315	0.33	0.55	42	1.593	1.681	0.088
Low	290	-0.35	0.10	72	1.649	1.586	–0.063

[a)]ref. [18]; [b)]Avg. $\phi = \cos^{-1}(\sqrt{\langle\cos^2\phi\rangle})$.

2.2. Elastic Anisotropy

We used BLS to characterize the elastic anisotropy of the three vapor-deposited glasses of itraconazole (Table 1) utilizing different scattering configurations to allow selection of both the direction and magnitude of the phonon wave vector, **q**. In order to illustrate the anisotropic elasticity, we first examine two orthogonal directions of **q** with respect to the glass film. In the transmission scattering geometry illustrated on the top of **Figure 2**a, **q** is directed parallel to the film and forming an angle, $\alpha = 90°$, relative to the film normal (x_3 axis) as the polarizations of incident and scattered light remain the same. The corresponding polarized (VV) BLS spectra (anti-Stokes side) of the three samples at $q = 0.0167$ nm^{-1} and 293 K are shown in the lower panel of Figure 2a; V denotes the polarization of light orthogonal to the scattering plane defined by the incident and scattered light beams, while H polarized light lies in the scattering plane. We note that the spurious frequency shifts induced by the collection of wide scattering wave vectors at large numerical apertures (NA > 0.2) are negligible in this work. This was confirmed by recording spectra at NA < 0.03 (Figure S1, Supporting Information). In the transmission scattering geometry, $q = (4\pi/\lambda)\sin(\theta/2)$ depends only on the scattering angle θ (Figure 2a), being independent of the sample's refractive index; $\lambda = 532$ nm is the laser wavelength in vacuum; and $\theta = 2\beta$. The phonon frequency f of the longitudinal (L) phonon mode is obtained from fitting single Lorentzian functions to the BLS spectra (solid lines). It is evident that the predominantly in-plane molecular orientation of the low T_{sub} sample is associated with the largest f among the three samples. This indicates that the longitudinal sound velocity is also the highest for this sample, calculated to be $v_L(\alpha = 90°) = 2\pi f/q = 2620 \pm 50$ m s^{-1}; for the high T_{sub}, $v_L(\alpha = 90°) = 2370 \pm 40$ m s^{-1}, being similar to the sound velocity $v_L(\alpha = 90°) = 2410 \pm 40$ m s^{-1} in the medium T_{sub} sample. This finding clearly shows that sound propagates with different speeds in molecular glasses of the same composition (i.e., itraconazole) but with different molecular orientations (Table 1). We verified the linear acoustic behavior of the

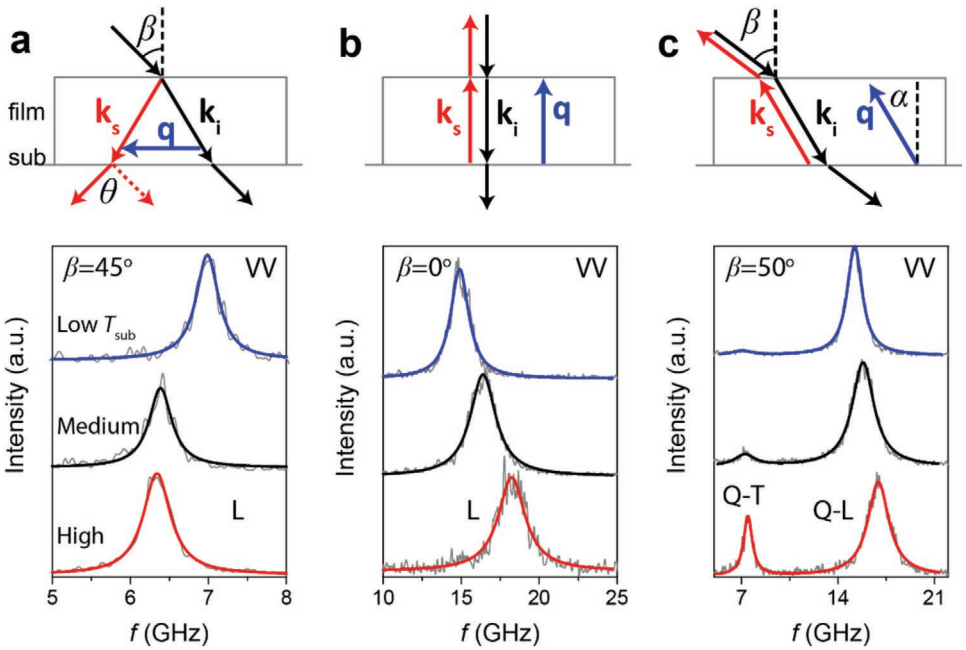

Figure 2. Typical polarized (VV) BLS spectra of the three itraconazole glasses corresponding to phonon wave vectors **q** directed a) parallel, b) perpendicular, and c) oblique to the film at VV configuration. The measurements in a) were conducted in the transmission geometry, whereas those in b) and c) were performed in the backscattering geometry. β and θ are the incident and scattering angle, receptively, and α denotes the direction of **q** relative to the film normal. In each geometry, $\mathbf{q} = \mathbf{k}_s - \mathbf{k}_i$, where $\mathbf{k}_i$ and $\mathbf{k}_s$ are the wave vectors of the incident and scattered light in the film. The magnitudes of the phonon wave vectors in a–c) can be calculated by Equations (S1)–(S2) (Supporting Information). The experimental spectra (gray lines) are fitted by Lorentzian functions (red, black, and blue lines). The observed peaks are assigned to longitudinal (L), quasi-longitudinal (Q-L), and quasi-transversal (Q-T) phonon modes as indicated in the three panels.

vapor-deposited glasses at GHz frequencies using two different values of q lying in-plane (Figure S2, Supporting Information). The observation that the speed of sound is independent of the magnitude of q confirms the absence of phonon dispersion at GHz frequencies.[21]

Figure 2b shows VV BLS spectra for the three itraconazole glasses for **q** parallel to the x_3 axis. This **q** direction can be realized in the backscattering configuration (at incident angle $\beta \approx 0°$ which is schematically shown on the top of Figure 2b). In contrast to the behavior shown in Figure 2a, for **q** parallel to the x_3 axis, the high T_{sub} film displays higher sound velocity $v_L(\alpha \approx 0°)$ than the low T_{sub} sample. It is evident that the predominantly vertical molecular orientation of the high T_{sub} sample is associated with the largest f of the longitudinal (L) phonon mode among the three samples. The longitudinal sound velocity, $v_L(\alpha \approx 0°) = 2\pi f/q = 3100 \pm 50$ m s^{-1}, is now the highest for the high T_{sub} sample, whereas for the medium (low) T_{sub}, $v_L(\alpha \approx 0°) = 2750 \pm 50$ (2410 ± 40) m s^{-1}, is distinctly slower. We note that in Figure 2b,c, $q = 4\pi n/\lambda$ depends on the refractive index n, which in the case of the VV-polarized backscattering spectra (Figure 2b,c) $n = n_o$ (Table 1, Section S1, Supporting Information).

The sound velocity ratio, $v_L(\alpha \approx 0°)/v_L(\alpha = 90°) = 1.31 \pm 0.03$ for the high T_{sub} implies an unexpectedly high elastic anisotropy considering reported measurements for molecular systems, as we discuss below. Given this result, we were surprised that, the low T_{sub} sample shows very low anisotropy, $v_L(\alpha = 90°)/v_L(\alpha \approx 0°) = 1.09 \pm 0.02$ in spite of significant molecular orientation parallel to the substrate (Figure 1, Table 1). Given the anisotropy trends observed in the longitudinal sound velocities at the two extreme directions ($\alpha = 0°$ or 90°), similar trends are anticipated for the pure-transverse (P-T) mode that can be resolved only in the depolarized (VH) BLS spectra; for the P-T mode, the directions of the phase and group velocities coincide. Indeed for in-plane propagation, the low T_{sub} sample displays the fastest $v_{P\text{-}T}(\alpha = 90°) = 1225 \pm 20$ m s^{-1} among the three samples (Figure S3, Supporting Information).

To achieve an unambiguous determination of the elastic tensor of the vapor-deposited itraconazole molecular glasses, we utilize the sample's symmetry to determine the necessary number of elastic constants. Vapor-deposited glasses of itraconazole can be considered as transverse isotropic materials with the x_3 axis being the symmetry axis. The transverse isotropy of vapor-deposited itraconazole molecular glasses has been verified in previous studies by IR absorbance[18] and GIWAXS measurements.[22] Transverse isotropy is confirmed in our BLS experiments by the constant sound velocities as the phonon wave vector **q** is directed in different in-plane directions (Figure S4, Supporting Information). While the molecular long axes can show substantial orientation with respect to the surface normal, as illustrated in Figure 1, the observed transverse isotropy means that the molecular long axes are oriented equally likely along any direction in the film plane.

For a transversely isotropic material,[12] the elastic tensor contains five independent elastic constants (herein chosen as C_{11}, C_{13}, C_{33}, C_{44}, and C_{66}), and it suffices to consider **q** vectors in a single plane containing the x_3 axis with α in the range of 0°–90° (Section S2, Supporting Information). Accordingly, we conducted BLS measurements at multiple incident angles in the backscattering geometry as illustrated on the top of Figure 2c, in addition to the experiments at extreme orientations ($\alpha = 0°$ or 90° in Figure 2a,b). Figure 2c shows VV spectra of the three samples recorded in the backscattering geometry with **q** forming an internal angle $\alpha \approx 29°$ relative to the x_3 axis. Two phonons, assigned to quasi-longitudinal (Q-L) and quasi-transverse (Q-T) modes, respectively, are observed in the spectra of the three samples; for the Q-L and Q-T modes, the directions of the phase and group velocities do not coincide. Note that the Q-T mode is detectable only in anisotropic materials as phonon propagates off the symmetry axis (Section S5, Supporting Information). Hence the appearance of Q-T modes in Figure 2c is an additional evidence of elasticity anisotropy in the three samples. The Q-L and Q-T modes at multiple α angles of high T_{sub} sample are shown in Figure S5a (Supporting Information), whereas the P-T modes resolved in the VH backscattering spectra are shown in Figure S5b (Supporting Information).

In order to describe the determination of the elastic constants from the direction-dependent sound velocities, we focus initially on the high T_{sub} sample as this sample exhibits the largest elastic anisotropy. The direction-dependent sound velocities of the high T_{sub} sample are plotted (symbols) in **Figure 3**a. The solid lines indicate the best fits according to a Christoffel-equation-based model (Equations (S7)–(S9), Supporting Information),[23] as discussed below. It is notable that the sound velocity of the Q-L mode, $v_{Q\text{-}L}$, in the high T_{sub} sample decreases monotonically from 3100 to 2370 m s^{-1} as α increases from 0° to 90° (Figure 3a). The sound velocity of the Q-T mode, $v_{Q\text{-}T}$, first increases, achieves a maximum at around $\alpha = 40°$–50°, and then decreases, which is a typical feature of $v_{Q\text{-}T}$ in transversely isotropic materials.[13,16,24] Unlike $v_{Q\text{-}L}$ and $v_{Q\text{-}T}$, the sound velocity of the P-T mode ($v_{P\text{-}T}$) shows a weak angular dispersion as $v_{P\text{-}T}$ assumes values almost equal to $v_{P\text{-}T}(\alpha = 90°)$. The robust nature of $v_{P\text{-}T}$ could be a general feature for soft matter, consistent with previous reports on collagen,[12] liquid crystal,[16] and spider silk.[24]

The experimental sound velocities of Figure 3a were analyzed by using a Christoffel-equation-based model (Equations (S7)–(S9), Supporting Information) through nonlinear χ^2 fitting (Section S2, Supporting Information) leading to a unique determination of the elastic stiffness constants (Table S1, Supporting Information). Based on the elastic stiffness constants, we calculated the engineering elastic moduli as listed in **Table 2** (Section 3). These are the Young's moduli in directions parallel and perpendicular to the x_3 axis ($E_{\parallel}$, $E_{\perp}$), shear moduli (G_{13}, G_{23}, G_{12}), bulk modulus (K), and Poisson's ratios (ν_{31}, ν_{32}, ν_{12}); these moduli are more relevant for applications than the elastic constants. The formulas and physical meanings of the elastic properties are summarized in Table S2 (Supporting Information). The uncertainties of the elastic properties were analyzed according to the principles of uncertainty propagation (Section S4, Supporting Information).[25]

The same procedure was used to determine the elastic constants and moduli for the medium T_{sub} and low T_{sub} itraconazole glasses. The experimental sound velocities in the medium T_{sub} sample (shown in Figure S6a, Supporting Information) display similar direction dependence as for the high T_{sub} sample (Figure 3a) although less pronounced; $v_L(\alpha \approx 0°)/v_L(\alpha = 90°) = 1.14$. The value of $v_{Q\text{-}L}$ is found to be insensitive to the direction of

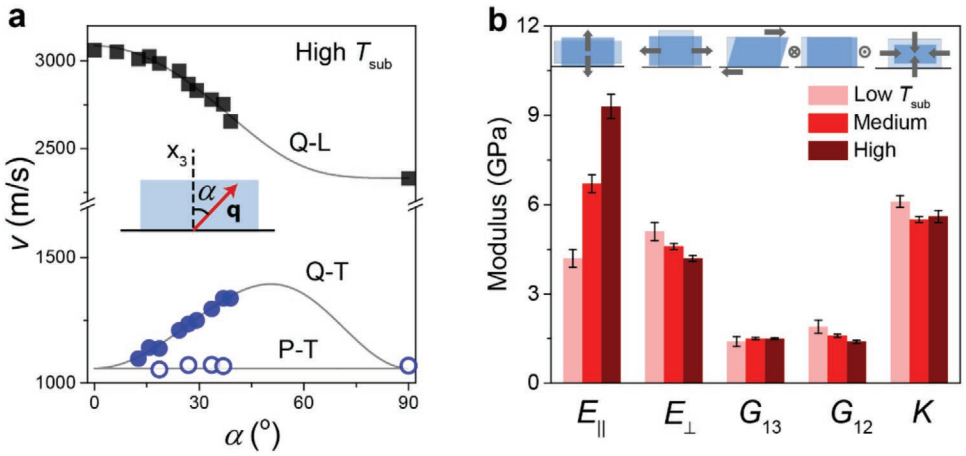

Figure 3. a) Direction-dependent sound velocities of the quasi-longitudinal (Q-L), quasi-transverse (Q-T), and pure-transverse (P-T) phonon modes in the high T_{sub} itraconazole glass. α is the angle between the phonon wave vector **q** and the x_3 axis (or film normal) as illustrated in the inset. The lines are best fits based on Equations (S7)-(S9) (Supporting Information). Experimental error is less than 2%. b) Young's ($E_{\|}$, $E_{\perp}$), shear (G_{13}, G_{23}, G_{12}), and bulk (K) moduli of the three itraconazole glasses. The schemes on the top illustrate the physical meanings of these moduli, which characterize the film's resistances to the external stresses indicated by the arrows. Note that $E_{\|}$ and $E_{\perp}$ represent Young's moduli parallel and normal to the x_3 axis, respectively.

α around the x_3 axis (Figure S4, Supporting Information), consistent with the previously-discussed transverse isotropy of the vapor-deposited itraconazole glasses. For the low T_{sub} sample with an orientation predominantly parallel to the substrate (Figure 1), $v_{Q\text{-}L}$ increases with α (Figure S6b, Supporting Information) but the variation with α is the smallest among the three samples. The engineering elastic moduli for the medium T_{sub} and low T_{sub} itraconazole glasses are listed in Table 2. As the phonon wavelength ($2\pi/q$) in these experiments is smaller than the sample thickness, the reported elastic constants and moduli are not influenced by the elastic properties of the substrate.[26]

Figure 3b compares the elastic moduli for the three itraconazole glasses. As T_{sub} decreases from 330 to 290 K, $E_{\|}$ decreases from 9.3 to 4.2 GPa, whereas $E_{\perp}$ increases from 4.2 to 5.1 GPa. Both of these observations indicate that the Young's modulus is highest when a sample is deformed along the molecular long axis direction as was reported earlier for covalently bonded polymers.[26] The mechanical anisotropy, $E_{\|}/E_{\perp}$, decreases from 2.2 to 0.8 with decreasing T_{sub}. As we discuss below, the high T_{sub} itraconazole glass displays the highest mechanical anisotropy known so far for molecular glasses.

Up to this point the analysis relied solely on the observed phonon frequencies. We note, however, that the intensity ratio, $I_{Q\text{-}T}/I_{Q\text{-}L}$, of the Q-T and Q-L modes in Figure 2c is different in the three samples and for the same sample also depends on the angle α (Figure S5, Supporting Information). To examine the consistency with our analysis of the elastic anisotropy, we consider the angular dependence of $I_{Q\text{-}T}/I_{Q\text{-}L}$, which is determined by the ratio of photoelastic coefficients P_{12} and P_{13} (Equation S17, Supporting Information).[27] In the case of the high T_{sub} sample, the increase of $I_{Q\text{-}T}/I_{Q\text{-}L}$ with angle α is represented by equation (S17, Supporting Information) using $P_{13}/P_{12} = 0.50 \pm 0.01$ (Figure S7, Supporting Information). For the medium T_{sub} and low T_{sub} samples, P_{13}/P_{12} are determined to 0.73 and 0.79, respectively. Thus the anticipated increase of P_{13}/P_{12} with decreasing mechanical anisotropy (Table 2) is consistent with the analysis of the sound velocity anisotropy and the trend conforms to the highest value, $P_{13}/P_{12} = 1$ and hence the disappearance of the Q-T mode ($I_{Q\text{-}T}/I_{Q\text{-}L} = 0$), in isotropic materials.

3. Discussion

These experiments on the vapor-deposited itraconazole glasses have produced two main results. First, the large Young's modulus anisotropy in the high T_{sub} sample ($E_{\|}/E_{\perp} \approx 2.2$) is unprecedented for molecular glasses. Second, when considering the three glasses together, there is a strong but nonlinear correlation between the Young's modulus (Figure 3b) and the average molecular orientation (Table 1). In this section, we place these results into the context of the previous work and deduce the relationship between the molecular orientation and elastic anisotropy for these glasses.

The large elastic anisotropy of the high T_{sub} itraconazole glass should be compared with reported values of other organic solids.

Table 2. Summary of elastic properties of the three itraconazole glasses. $E_{\|}$, $E_{\perp}$: axial, lateral Young's modulus (GPa); G_{13}, G_{23}, G_{12}: shear moduli (GPa); K: bulk modulus (GPa); ν_{31}, ν_{32}, ν_{12}: Poisson's ratio.

Sample	$E_{\|}$	$E_{\perp}$	$E_{\|}/E_{\perp}$	$G_{13/23}$	G_{12}	K	$\nu_{31/32}$	ν_{12}
High T_{sub}	9.3 ± 0.4	4.2 ± 0.1	2.2	1.50 ± 0.03	1.40 ± 0.05	5.6 ± 0.2	0.37 ± 0.02	0.51 ± 0.03
Medium T_{sub}	6.7 ± 0.3	4.6 ± 0.1	1.5	1.50 ± 0.04	1.60 ± 0.06	5.5 ± 0.1	0.36 ± 0.02	0.43 ± 0.03
Low T_{sub}	4.2 ± 0.3	5.1 ± 0.3	0.8	1.40 ± 0.15	1.90 ± 0.21	6.1 ± 0.2	0.35 ± 0.02	0.35 ± 0.09

For noncrystalline solids, the most relevant comparisons are rod-like liquid crystals. The elastic anisotropy reported for liquid crystals is relatively small in spite of their strong optical anisotropy.[28,29] The sound velocity in the nematic and smectic phases is anisotropic, but $v_L(\alpha \approx 0°)/v_L(\alpha = 90°)$ is within 5% of unity at hypersonic frequencies.[30–32] The largest value of $v_L(\alpha \approx 0°)/v_L(\alpha = 90°)$ that we found in the literature is 1.05 for 4′-octyl-4-biphenylcarbonitrile (8CB) liquid crystals in the smectic phase.[33,34] This is much smaller than the values (e.g., 1.31 for the high T_{sub} sample) for the itraconazole glasses presented in this work. It is not clear to us why itraconazole glasses have a larger elastic anisotropy than other liquid crystals. Itraconazole has a more rigid molecular structure than 8CB and this may be an important factor. The present measurements were performed in the glassy state, while previous measurements on liquid crystals have generally been performed above the glass transition temperature T_g. We do not expect that this should influence the elastic anisotropy comparison since all these measurements are performed in the high frequency limit in which the samples respond as an elastic solid, even though the isotropic elasticity decreases with increasing temperature above T_g.[35] However, we are not aware of any literature report on the elastic anisotropy of a material in both the glassy and liquid states, so such a comparison is an important target for future work. If many liquid crystals have large mechanical anisotropies in the glassy state, this would provide an important source of materials for investigations targeting a fundamental understanding of mechanical anisotropy.

Even when we extend the comparison of the elastic anisotropy to crystalline and partially crystalline materials, the elastic anisotropy of the high T_{sub} itraconazole glass is remarkably high. For spider silk fibers,[24] $E_{\parallel}/E_{\perp} \approx 2$ is slightly lower than that for the High T_{sub} itraconazole glass. It is interesting that even this highly oriented and partially crystalline material (crystallinity: ≈22%) has a similar elastic anisotropy as the high T_{sub} itraconazole sample. For organic molecular crystals, such as saccharin,[36] aspirin,[37,38] and cyclotrimethylenetrinitramine (RDX),[39] the largest ratio of the elastic moduli along different crystal faces is usually less than 2.[40–43] For instance, the wave-like π-stacked energetic crystals of 1,1-diamino-2,2-dinitroethylene (FOX-7) show a mechanical anisotropy $E_{(002)}/E_{(020)} = 1.9$.[44] For a two-component hybrid Bragg stack composed of alternating inorganic (hectorite) and polymer (polyvinylpyrrolidone)[13] layers, the elastic anisotropy ($E_{\parallel}/E_{\perp}$) can be as high as 7 and this is the highest reported value so far for hybrid nanocomposites. This hybrid Bragg stack, however, is a two-component system; the moduli of the two pure materials differ by roughly an order of magnitude and this likely has an important influence on the elastic anisotropy of the hybrid stack.

This work provides the first opportunity to investigate the connection between molecular orientation and elastic anisotropy in molecular glasses. **Figure 4** shows the nonlinear dependence of $E_{\parallel}$ and $E_{\perp}$ (Table 2) on the molecular orientation order parameter S_z (Table 1). The strong correlation between $E_{\parallel}$ and S_z is qualitatively reasonable. For a sample in which all the molecular long axes point in nearly the same direction (such as the high T_{sub} glass), the Young's modulus along the long axes of the itraconazole molecules should be higher, as covalent bonds are more difficult to stretch than van der Waals contacts.[26] In the perpendicular direction, the high T_{sub} glass is the easiest to stretch as this involves primarily van der Waals contacts. As S_z decreases, a greater fraction of molecular long axes lie in the film plane and the resistance to in-plane deformation increases as it is difficult to stretch these covalent bonds, leading to an increased $E_{\perp}$. Since only a fraction of the molecular long axes lie in the direction of deformation (as a result of transverse isotropy), the maximum value of $E_{\perp}$ is relatively modest. Analogously, it was recently reported that thermal conductivity in vapor-deposited glasses is also correlated with molecular orientation, with the most efficient thermal transport occurring along the molecular long axes.[45]

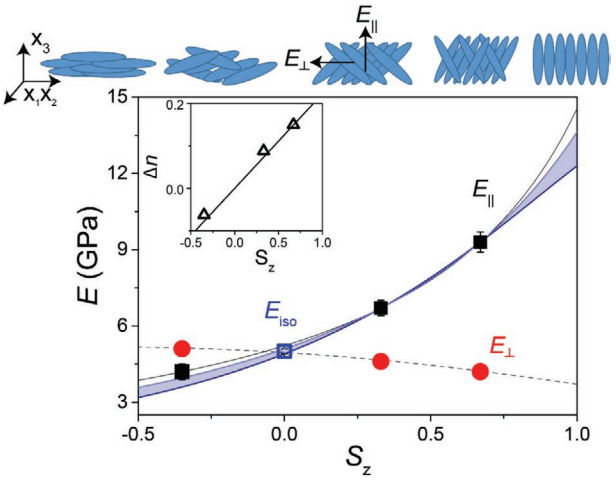

Figure 4. $E_{\parallel}$ (solid black) and $E_{\perp}$ (solid red) for the three itraconazole glasses as a function of the S_z order parameter along with schematics of glass structures on the top. The shaded area line is the representation by Equation (2) of $E_{\parallel}(S_z)$ in the high and medium T_{sub} samples and E_{iso} ($S_z = 0$) (open square). The black line denotes the fit of Equation (2) to $E_{\parallel}(S_z)$ for all three samples. The grey dash line connecting $E_{\perp}$ is a guide for the eye. Inset: The linear relation between birefringence Δn and S_z for the three glasses.

As there is no theoretical expression for $E_{\parallel}$ as a function of S_z, we derive one based upon the following heuristic argument. We recall that $E_{\parallel}$ was obtained from the representation of $v(\alpha)$ (Figure 3a), whereas $S_z = [3\langle\cos^2\phi\rangle - 1]/2$ refers to the average orientation angle ϕ of the molecular long axis $\hat{\boldsymbol{n}}$. The direction-dependent Young's modulus $E_{\parallel}(\phi)$ obtained from the continuum mechanics analysis for transversely isotropic materials is given by Equation (1)

$$E_{\parallel}(\phi) = \left[\frac{\sin^4\phi}{E_{\perp}^*} + \left(\frac{1}{G_{23}^*} - \frac{2\nu_{31}^*}{E_{\parallel}^*}\right)\sin^2\phi\cos^2\phi + \frac{\cos^4\phi}{E_{\parallel}^*}\right]^{-1} \quad (1)$$

where the elastic parameters, $E_{\perp}^*, E_{\parallel}^*, G_{23}^*$ and ν_{31}^*, refer to the perfect orientation with $\phi = 0°$. Assuming $\langle\cos^2\phi\rangle = \cos^2\phi$ and substituting ϕ by S_z, Equation (1) can be written as

$$E_{\parallel}(S_z) = \left(aS_z^2 + bS_z + c\right)^{-1} \quad (2)$$

where a, b, and c are parameters related to $E_{\perp}^*, E_{\parallel}^*, G_{23}^*$ and we utilize this form to fit the data in Figure 4.

Since Equation (2) has three unknowns, the $E_{\parallel}(S_z)$ values for at least three equivalent samples, distinguished only by the orientation parameter, is required. In the case of the low T_{sub}

sample, however, the density is higher by about 0.4% than for the other two samples. Previous measurements have shown that density can change the modulus even for isotropic glasses; a density increase of 1.2% can lead to about 15% higher Young's modulus.[35] For the low T_{sub} sample, $E_{||}(S_z = -0.35)$ is expected to be ≈5% higher than for a sample with the same orientation but lower density and is therefore not equivalent to the other two samples in the context of Equation (2). However, we can estimate that an isotropic itraconazole glass would have $E_{iso}(S_z = 0) = 5.0 \pm 0.1$ GPa; we obtain this value from a linear extrapolation of $E_{\perp}$ for the high and medium T_{sub} samples (Table 2). The shaded area in Figure 4 indicates fits of Equation (2) to the $E_{||}(S_z)$ values for the high and medium T_{sub} samples together with E_{iso}. We note that the experimental $E_{||}(S_z = -0.35)$ in the low T_{sub} sample is higher than predicted by Equation (2), consistent with the above comments about density. For comparison, the black solid line shows the result if $E_{||}(S_z)$ for the three samples is fit to Equation (2), without utilizing the isotropic value. In this case, the isotropic $E_{iso}(S_z = 0) = 5.2$ GPa value is slightly (4%) higher than the estimated (open square) value from the $E_{\perp}$ in the high and medium T_{sub} samples.

We can use the fitted data in Figure 4 to estimate the elastic anisotropy of itraconazole glasses that are even more highly ordered than those studied in this work. Based upon the fits shown by the shaded area in Figure 4, we estimate that for perfectly oriented samples, $E_{||}(S_z = 1)$ is 13.0 ± 0.6 GPa. From the linear fit to $E_{\perp}$ (Table 2), we estimate $E_{\perp}(S_z = 1)$ is 3.8 ± 0.2 GPa. Based on these values, the mechanical anisotropy $E_{||}/E_{\perp} = 3.4 \pm 0.3$ for a perfectly orientated itraconazole sample, a value that is considerably higher than observed for the high T_{sub} sample ($S_z = 0.67$). As a final check on the reliability of the comparisons shown in Figure 4, we show a graph of the birefringence Δn of the three samples as a function of S_z in the inset of this figure.[18,46] The validity of this linear $\Delta n(S_z)$ relation through the origin for the three samples provides confidence that the relationship $E_{||}(S_z)$ in Figure 4 is significant.

Although we do not know if the behavior shown in Figure 4 is general for molecular glasses, we anticipate that Equation (2) for $E_{||}$ will have general utility. Equation (2) predicts that two glasses with the same orientational order but with different amounts of smectic layering will have the same elastic anisotropy, and it would be useful to test this directly. We expect that computer simulations will be useful to explore the connection between molecular orientation, smectic structure, and elastic anisotropy.

Finally, we comment on additional quantitative features of the moduli measured here for the three itraconazole glasses. The shear moduli and bulk modulus assume values typical for polymer[26] and molecular glasses.[35] The shear modulus G_{23} (Table 1) that describes deformation along the x_1–x_2 plane is very similar for the three samples. The Poisson's ratios for all the itraconazole glasses show values typical of molecular glasses[35,47] ($\nu \approx 0.36$) with the exception of ν_{12} for the High T_{sub} glass which has the surprisingly high value of 0.50, a value that is typical of the liquid state.

4. Conclusions

While previous work has characterized anisotropic molecular orientation in vapor-deposited glasses, the present work explored the elastic anisotropy of such glasses for the first time. Micro-Brillouin light spectroscopy is ideally suited for this investigation, as changing the angle of the scattering wave vector relative to the substrate normal allows a complete determination of the elastic stiffness tensor. The itraconazole glass deposited at the highest substrate temperature, which features predominantly vertical molecular orientation, exhibited a remarkably high value (≈2.2) for the ratio of the out-of-plane and in-plane Young's moduli. The elastic anisotropy for this sample is much larger than values previously observed for liquid crystals and is larger than those observed for many 3D crystals. For glasses of itraconazole, we find a strong correlation between molecular orientation and elastic anisotropy implying that deformation along the long molecular axis of itraconazole is subject to a higher modulus. It was previously shown that vapor-deposited itraconazole glasses have kinetic stabilities equal to or exceeding a liquid-cooled glass,[48] indicating that glasses can simultaneously be mechanically anisotropic and kinetically stable.

We presented a general equation connecting the molecular orientation and elastic anisotropy, and we expect that this will have utility for many molecular glasses. For applications in organic electronics, where it may be important to control the in-plane modulus, this equation provides a means of predicting elastic properties based upon a few experimental measurements. For itraconazole, this equation indicates that it may be possible to produce molecular glasses in which the ratio of the out-of-plane and in-plane Young's moduli exceeds three, if sufficiently high molecular orientation can be achieved. It will be important to investigate the elastic anisotropy of additional molecular systems, including organic semiconductors, to understand whether similarly anisotropic mechanical properties are observed.

5. Experimental Section

All experiments and methods are described in detail in the Supporting Information.

Supporting Information

Supporting Information is available from the Wiley Online Library or from the author.

Acknowledgements

Y.C. and Z.W. contributed equally to this work. Y.C., Z.W., and G.F. acknowledge the financial support by ERC AdG SmartPhon (Grant No. 694977). Sample preparation, GIWAXS, and ellipsometry was supported by NSF through the University of Wisconsin Materials Research Science and Engineering Center (DMR-1720415) for C.B., L.Y., and M.E. Use of the Stanford Synchrotron Radiation Lightsource, SLAC National Accelerator Laboratory, is supported by the U.S. Department of Energy, Office of Science, Office of Basic Energy Sciences under Contract No. DE-AC02-76SF00515.

Conflict of Interest

The authors declare no conflict of interest.

Keywords

Brillouin light spectroscopy, elastic anisotropy, molecular glasses, orientation, vapor deposition

Received: February 15, 2020
Published online:

[1] M. D. Ediger, J. de Pablo, L. Yu, *Acc. Chem. Res.* **2019**, *52*, 407.
[2] J. Rafols-Ribe, P. A. Will, C. Hanisch, M. Gonzalez-Silveira, S. Lenk, J. Rodriguez-Viejo, S. Reineke, *Sci. Adv.* **2018**, *4*, eaar8332.
[3] D. Yokoyama, *J. Mater. Chem.* **2011**, *21*, 19187.
[4] B. J. Boehm, H. T. Nguyen, D. M. Huang, *J. Phys.: Condens. Matter* **2019**, *31*, 423001.
[5] W. Pisula, M. Zorn, J. Y. Chang, K. Müllen, R. Zentel, *Macromol. Rapid Commun.* **2009**, *30*, 1179.
[6] S. F. Swallen, K. L. Kearns, M. K. Mapes, Y. S. Kim, R. J. McMahon, M. D. Ediger, T. Wu, L. Yu, S. Satija, *Science* **2007**, *315*, 353.
[7] S. S. Dalal, D. M. Walters, I. Lyubimov, J. J. de Pablo, M. D. Ediger, *Proc. Natl. Acad. Sci. USA* **2015**, *112*, 4227.
[8] D. M. Walters, L. Antony, J. J. de Pablo, M. D. Ediger, *J. Phys. Chem. Lett.* **2017**, *8*, 3380.
[9] A. Gujral, J. Goomez, S. G. Ruan, M. F. Toney, H. Bock, L. Yu, M. D. Ediger, *Chem. Mater.* **2017**, *29*, 9110.
[10] K. Bagchi, N. E. Jackson, A. Gujral, C. Huang, M. F. Toney, L. Yu, J. J. de Pablo, M. D. Ediger, *J. Phys. Chem. Lett.* **2019**, *10*, 164.
[11] M. A. Reyes-Martinez, A. Ramasubramaniam, A. L. Briseno, A. J. Crosby, *Adv. Mater.* **2012**, *24*, 5548.
[12] S. Cusack, A. Miller, *J. Mol. Biol.* **1979**, *135*, 39.
[13] Z. Wang, K. Rolle, T. Schilling, P. Hummel, A. Philipp, B. A. F. Kopera, A. M. Lechner, M. Retsch, J. Breu, G. Fytas, *Angew. Chem., Int. Ed.* **2020**, *59*, 1286.
[14] C. Tangpatjaroen, K. Bagchi, R. A. Martinez, D. Grierson, I. Szlufarska, *J. Phys. Chem. C* **2018**, *122*, 27775.
[15] N. Iguiñiz, R. Frisenda, R. Bratschitsch, A. Castellanos-Gomez, *Adv. Mater.* **2019**, *31*, 1807150.
[16] M. Ryu, Y. Cang, Z. Wang, G. Fytas, J. Morikawa, *J. Phys. Chem. C* **2019**, *123*, 17148.
[17] B. Graczykowski, M. Sledzinska, M. Placidi, D. Saleta Reig, M. Kasprzak, F. Alzina, C. M. Sotomayor Torres, *Nano Lett.* **2017**, *17*, 7647.
[18] J. Gomez, J. Jiang, A. Gujral, C. Huang, L. Yu, M. D. Ediger, *Soft Matter* **2016**, *12*, 2942.
[19] C. Bishop, J. L. Thelen, E. Gann, M. F. Toney, L. Yu, D. M. DeLongchamp, M. D. Ediger, *Proc. Natl. Acad. Sci. USA* **2019**, *116*, 21421.
[20] M. Tarnacka, K. Adrjanowicz, E. Kaminska, K. Kaminski, K. Grzybowska, K. Kolodziejczyk, P. Wlodarczyk, L. Hawelek, G. Garbacz, A. Kocot, M. Paluch, *Phys. Chem. Chem. Phys.* **2013**, *15*, 20742.
[21] P. Voudouris, N. Gomopoulos, A. L. Grand, N. Hadjichristidis, G. Floudas, M. D. Ediger, G. Fytas, *J. Chem. Phys.* **2010**, *132*, 074906.
[22] A. Gujral, J. Gomez, J. Jiang, C. B. Huang, K. A. O'Hara, M. F. Toney, M. L. Chabinyc, L. Yu, M. D. Ediger, *Chem. Mater.* **2017**, *29*, 849.
[23] M. Mah, D. Schmitt, *Geophysics* **2001**, *66*, 1217.
[24] Z. Wang, Y. Cang, F. Kremer, E. L. Thomas, G. Fytas, *Biomacromolecules* **2020**, *21*, 1179.
[25] M. Zgonik, P. Bernasconi, M. Duelli, R. Schlesser, P. Gunter, M. H. Garrett, D. Rytz, Y. Zhu, X. Wu, *Phys. Rev. B* **1994**, *50*, 5941.
[26] N. Gomopoulos, G. Saini, M. Efremov, P. F. Nealey, K. Nelson, G. Fytas, *Macromolecules* **2010**, *43*, 1551.
[27] C. Hamaguchi, *J. Phys. Soc. Jpn.* **1973**, *35*, 832.
[28] D. G. Gleed, J. R. Sambles, G. W. Bradberry, *Phys. Rev. A* **1989**, *134*, 440.
[29] K. Miyano, J. B. Ketterson, in *Physical Acoustics*, Vol. *14* (Eds.: W. P. Mason, R. N. Thurston), Academic Press, San Diego, CA **1979**, pp. 93–178.
[30] Y. Liao, N. A. Clark, P. S. Pershan, *Phys. Rev. Lett.* **1973**, *30*, 639.
[31] A. Wergin, W. Krasser, H. H. Stiller, C. G. B. Frischkorn, *Phys. Rev. A* **1979**, *20*, 1120.
[32] M. E. Mullen, M. J. Stephen, B. Luthi, *Phys. Rev. Lett.* **1972**, *28*, 799.
[33] D. G. Gleed, J. R. Sambles, G. W. Bradberry, *Liq. Cryst.* **1988**, *3*, 1689.
[34] G. W. Bradberry, C. F. Clarke, *Phys. Rev. A* **1983**, *95*, 305.
[35] K. L. Kearns, T. Still, G. Fytas, M. D. Ediger, *Adv. Mater.* **2010**, *22*, 39.
[36] M. S. R. N. Kiran, S. Varughese, C. M. Reddy, U. Ramamurty, G. R. Desiraju, *Cryst. Growth Des.* **2010**, *10*, 4650.
[37] D. Olusanmi, K. J. Roberts, M. Ghadiri, Y. Ding, *Int. J. Pharm.* **2011**, *411*, 49.
[38] S. Varughese, M. S. R. N. Kiran, K. A. Solanko, A. D. Bond, U. Ramamurty, G. R. Desiraju, *Chem. Sci.* **2011**, *2*, 2236.
[39] K. J. Ramos, D. E. Hooks, D. F. Bahr, *Philos. Mag.* **2009**, *89*, 2381.
[40] S. Varughese, M. S. Kiran, U. Ramamurty, G. R. Desiraju, *Angew. Chem., Int. Ed.* **2013**, *52*, 2701.
[41] S. Mannepalli, K. S. R. N. Mangalampalli, *Crystals* **2017**, *7*, 324.
[42] R. Folland, D. Jackson, S. Rajagopal, *Mol. Phys.* **1975**, *30*, 1053.
[43] A. Yoshihara, E. R. Bernstein, *J. Chem. Phys.* **1982**, *77*, 5319.
[44] X. Q. Zhou, Z. P. Lu, Q. Zhang, D. Chen, H. Z. Li, F. D. Nie, C. Y. Zhang, *J. Phys. Chem. C* **2016**, *120*, 13434.
[45] J. Ràfols-Ribé, R. Dettori, P. Ferrando-Villalba, M. Gonzalez-Silveira, L. Abad, A. F. Lopeandía, L. Colombo, J. Rodríguez-Viejo, *Phys. Rev. Mater.* **2018**, *2*, 035603.
[46] I. Ward, *Br. J. Appl. Phys.* **1967**, *18*, 1165.
[47] E. Lerner, *J. Non-Cryst. Solids* **2019**, *522*, 119570.
[48] J. Gómez, A. Gujral, C. Huang, C. Bishop, L. Yu, M. D. Ediger, *J. Chem. Phys.* **2017**, *146*, 054503.